

Anisotropic physical properties and large critical current density in $\text{KCa}_2\text{Fe}_4\text{As}_4\text{F}_2$ single crystal

Sunseng Pyon¹, Yuto Kobayashi¹, Ayumu Takahashi¹, Wenjie Li¹, Teng Wang², Gang Mu², Ataru Ichinose³, Tadashi Kambara⁴, Atsushi Yoshida⁴, Tsuyoshi Tamegai¹

1 Department of Applied Physics, The University of Tokyo, 7-3-1 Hongo, Bunkyo-ku, Tokyo 113-8656, Japan

2 State Key Laboratory of Functional Materials for Informatics, Shanghai Institute of Microsystem and Information Technology, Chinese Academy of Sciences, Shanghai 200050, China

3 Central Research Institute of Electric Power Industry, Electric Power Engineering Research Laboratory, 2-6-1, Nagasaka, Yokosuka-shi, Kanagawa 240-0196, Japan

4 Nishina Center, RIKEN, 2-1 Hirosawa, Wako, Saitama 351-0198, Japan

Abstract

We present a systematic study of electrical resistivity, Hall coefficient, magneto-optical imaging, magnetization, and STEM analyses of $\text{KCa}_2\text{Fe}_4\text{As}_4\text{F}_2$ single crystals. Sharp diamagnetic transition and magneto-optical imaging reveal homogeneity of single crystal and prominent Bean-like penetrations of vortices. Large anisotropy of electrical resistivity, with $\rho_c/\rho_{ab} > 100$, and semiconductor-like ρ_c suggest that the electronic state is quasi two-dimensional. Hall effect measurements indicate that $\text{KCa}_2\text{Fe}_4\text{As}_4\text{F}_2$ is a multiband system with holes as main carriers. Magnetization measurements reveal significantly larger J_c compared with that in other iron-based superconductors with different values of J_c depending on the direction of magnetic field. Origin of these J_c characteristics is discussed based on microstructural observations using STEM. In addition, further enhancement of J_c in $\text{KCa}_2\text{Fe}_4\text{As}_4\text{F}_2$ for future application is demonstrated in terms of heavy-ion irradiation.

Introduction

The discovery of iron-based superconductors (IBSs) in 2008 [1] has prompted great interest in the field of condensed matter physics. Their multi-gap superconductivity due to their multiband electronic structures were studied. Not only their unconventional superconducting mechanism leading to high transition temperature, but also their potential for applications has been extensively studied and several types of IBSs are expected as candidates for future applications [2,3,4]. In the case of widely-studied IBSs such as 122-type $(\text{Ba,K})\text{Fe}_2\text{As}_2$ [5], their electronic states are three-dimensional with weak anisotropy. It makes good a contrast to two-dimensional electronic states in cuprate superconductors. Recently, however, it is suggested that quasi two-dimensional electronic states emerge in novel IBSs such as 12442-type compounds [6-10] or some IBSs consisting of FeSe layers sandwiched by thick insulating layers [11,12]. The 12442-type IBSs, a series of bi-layered compounds $AB_2\text{Fe}_4\text{As}_4\text{C}_2$ ($A = \text{K, Rb, and Cs}$; $B = \text{Ca, Nd, Sm, Gd, Tb, Dy, and Ho}$; and $C = \text{F and O}$) are recognized as the intergrowth of 1111- and 122-type IBSs, and reported to be superconductors with superconducting transition temperature $T_c = 28\text{--}37\text{ K}$ [6-10]. The 12442-type IBSs have double Fe_2As_2 conducting layers between two neighboring Ca_2F_2 insulating layers [6]. Based on the first-principle calculation, 10 bands crossing the Fermi level are predicted, which are more complicated than other IBSs, showing multi-band character [12]. Using polycrystalline samples of 12442-type IBSs, their electronic and magnetic structures have been investigated [14-16]. Furthermore, very recently, the growth of millimeter-sized high-quality single crystals of 12442-type IBSs was reported [17,18]. It is needless to say that studies on high-quality single crystals are essential to reveal intrinsic properties of these superconductors. Using these single crystals, electronic states with large anisotropy were revealed by the estimation of the upper critical field, H_{c2} [17,18], and torque analyses [19]. In addition, neutron spin resonance measurements revealed quasi two-dimensional electronic behavior of $\text{KCa}_2\text{Fe}_4\text{As}_4\text{F}_2$, which is similar to those of highly anisotropic cuprate superconductors [20]. Not only elucidation of unconventional superconductivity but also the possibility of future application of this material is intriguing topics. H_{c2} of $\text{KCa}_2\text{Fe}_4\text{As}_4\text{F}_2$ is much larger than that of other systems of IBSs, when the magnetic field is applied along the ab plane, and large anisotropy parameter $\gamma (= H_{c2}^{ab}/H_{c2}^c) \sim 8$ was revealed near the superconducting transition [17,21,22]. Large H_{c2} is helpful for future high-field applications. Although critical current density, J_c , in $\text{KCa}_2\text{Fe}_4\text{As}_4\text{F}_2$ has not been reported yet, recent report on J_c in $\text{CsCa}_2\text{Fe}_4\text{As}_4\text{F}_2$ at 2 K under self-field is comparable to that in well-studied 122-type materials [18,23]. Further studies on J_c in 12442-type IBSs are demanded.

In this paper, we characterize the superconducting properties of $\text{KCa}_2\text{Fe}_4\text{As}_4\text{F}_2$ single crystals by measuring anisotropic electrical resistivity, in-plane Hall coefficient, and anisotropic irreversible magnetization. The quality and microstructure of single crystals were also characterized by magneto-optical imaging and scanning transmission electron microscopy (STEM). The electronic

structure of $\text{KCa}_2\text{Fe}_4\text{As}_4\text{F}_2$ is discussed by comparing it with that in other IBSs. In addition, we found significantly large in-plane J_c in $\text{KCa}_2\text{Fe}_4\text{As}_4\text{F}_2$ compared with that in other IBSs, and unique anisotropy of J_c depending on the direction of magnetic field. Further enhancement of J_c in $\text{KCa}_2\text{Fe}_4\text{As}_4\text{F}_2$ for future application in terms of heavy-ion irradiation is also demonstrated.

Experimental methods

Single crystals of $\text{KCa}_2\text{Fe}_4\text{As}_4\text{F}_2$ were grown using the self-flux method with KAs as flux. Details of sample growth and basic physical properties have been reported in ref. [17]. The bulk magnetization for $H \parallel c$ -axis and ab -plane were measured to evaluate the J_c by using a superconducting quantum interference device (SQUID) magnetometer (MPMS-5XL, Quantum Design). Electrical resistivity along the ab -plane (ρ_{ab}) and along the c -axis (ρ_c) were measured by the four-probe method. Anticipating relatively large anisotropy of transport properties based on the previous measurements [17], care was taken to prepare electrical contacts so that the current flows uniformly. In the case of ρ_{ab} measurement, consistency of the values evaluated on the top and bottom surfaces was carefully examined. The Hall voltage was measured with a Quantum Design physical property measurement system (PPMS) with the AC transport option with current density of $\sim 11 \text{ A/cm}^2$. The Hall voltage was obtained from the antisymmetric part of transverse voltage by subtracting the positive and negative magnetic field data. Macroscopic homogeneity of superconductivity was examined by measuring the critical state field profile using magneto-optical (MO) imaging. For MO imaging, an iron-garnet indicator film was placed in direct contact with the sample surface, and the whole assembly was attached to the cold finger of a He-flow cryostat (Microstat-HR, Oxford Instruments). MO images were acquired by using a cooled-CCD camera with 12-bit resolution (ORCA-ER, Hamamatsu). Cross-sectional observations of the single crystals were performed with a high-resolution STEM (JEOL, JEM-2100F). Enhancement of J_c was attempted by irradiating 2.6 GeV U ion along the c -axis at RIKEN Ring Cyclotron in RI Beam Factory operated by RIKEN Nishina Center and CNS, The University of Tokyo. Columnar defects at a dose-equivalent matching fields of $B_\Phi = 40 \text{ kG}$ were created.

Results and discussions

Figure 1 shows the temperature dependence of magnetization ($H \parallel c$ -axis) at 5 Oe for $\text{KCa}_2\text{Fe}_4\text{As}_4\text{F}_2$ ($510 \times 390 \times 7.8 \text{ } \mu\text{m}^3$). T_c defined by the onset of diamagnetism is 33.0 K and ΔT_c is less than 1 K. The quality of the sample is almost the same as that reported in the previous publication [17].

MO imaging of $\text{KCa}_2\text{Fe}_4\text{As}_4\text{F}_2$ was performed to evaluate its homogeneity and quality. Figures 2(a) and 2(b) display MO images of $\text{KCa}_2\text{Fe}_4\text{As}_4\text{F}_2$ in the remanent state at (a) 5 K and (b) 20 K, respectively, after cycling the field up to 1.2 kOe for 0.2 s. The crystal for MO measurements are

carefully cut into a parallelepiped with smooth surface and no visible cracks as shown in the optical micrograph of Fig. 2(c). At 5 K, the magnetic field is mostly shielded and only partially penetrates the sample due to large J_c and the limitation of the value of the applied field. A faint horizontal white line near the center of the crystal may indicate a small crack which is invisible from the surface. At 20 K, the magnetic field reaches the center of the sample and the MO image of the right part shows the critical state field profile expected for a uniform thin-plate superconductor with clear current-discontinuity lines (d lines), although the magnetic field in the left half of the sample is not fully penetrated. These results indicate that the sample is fairly homogeneous with a weak variation of J_c in the crystal. Local magnetic induction profiles at different temperatures taken along the broken line in Fig. 2(a) are shown in Fig. 2(d). Magnetic induction profiles at higher temperatures of 20~30 K show rooftop patterns, indicating that the large and homogeneous current flows throughout the sample. At lower temperatures, however, the magnetic induction at the center of the sample are almost zero, since J_c in the sample is so high that the applied field up to 1.2 kOe is shielded. From the value of the trapped field, J_c can be roughly evaluated [24]. At 20 K, trapped magnetic induction ΔB is 581 G. Using the approximate formula between ΔB and J_c for a thin superconductor with a thickness t , $J_c \sim \Delta B / (t * \beta)$, with $t = 9 \mu\text{m}$ (β is a parameter determined by the sample dimensions and the distance between the sample surface and the garnet film, and $\beta \sim 3.3$ in the present case) [24], J_c at 20 K under the self-field is evaluated as 0.19 MA/cm^2 .

The superconducting transition and electrical characteristics are also evaluated by the temperature dependence of ρ_{ab} . Two kinds of samples, No. 1 ($920 \times 392 \times 8 \mu\text{m}^3$) and No. 2 ($878 \times 236 \times 3 \mu\text{m}^3$) with different contact configurations are measured. The contact configuration for the sample No. 1 and No. 2 are shown in Fig. 3(a). Temperature dependences of ρ_{ab} of the two samples are shown in Fig. 3(b). The absolute value of $\rho_{ab} \sim 300 \mu\Omega\text{cm}$ at room temperature and their temperature dependences are consistent with each other. Both sample show sharp superconducting transitions at $\sim 34.0 \text{ K}$. When the electrical resistivity of anisotropic crystals is evaluated, it is possible that the resistivity is estimated incorrectly due to inhomogeneous current flow, in particular along the direction perpendicular to the surface. However, the fact that ρ_{ab} of sample No. 2, where voltage contacts are attached on the opposite surface to the current contacts agrees with that of sample No. 1 with all contacts on the same surface, suggest that we can ignore the possible error in the absolute value of ρ_{ab} due to sample inhomogeneity and anisotropy. As shown in Fig. 3(b), $\rho_{ab}(T)$ shows a tendency of saturation with increasing temperature. Similar saturating behaviors are also observed such as in K-doped BaFe_2As_2 [25], or $\text{CaKFe}_4\text{As}_4$ [26,27], and values of ρ_{ab} at room temperature are very similar. In general, an electrical resistivity is inversely proportional to the mean free path of electrons l in metals. As Ioffe and Regel argued, metallic conduction occurs only when l is larger than the interatomic spacing a [28]. So maximum resistivity is limited, and that is maximized when l is comparable to a . This limit known as Mott–Ioffe–Regel (MIR) limit is universally observed in

several metals, and the values of saturated resistivity around 100-400 $\mu\Omega\text{cm}$ were reported [29]. By considering similarity of $\rho_{ab}(T)$ and lattice parameter between $\text{KCa}_2\text{Fe}_4\text{As}_4\text{F}_2$ and K-doped BaFe_2As_2 or $\text{CaKFe}_4\text{As}_4$, $\rho_{ab} \sim 300 \mu\Omega\text{cm}$ at room temperature is more plausible than that $\sim 1.3 \text{ m}\Omega\text{cm}$ in previous report [17]. We tried to estimate the residual resistivity at 0 K, $\rho(0 \text{ K})$, by curve fitting using the equation $\rho(T) = \rho(0 \text{ K}) + A_1T + A_2T^2$ and $\rho(T) = \rho(0 \text{ K}) + AT^n$, over the range of 40 to 80 K to evaluate the sample quality. We observed negative $\rho(0 \text{ K})$ values obtained by these two fittings due to the relatively large T -linear contribution in this temperature range. Similar negative $\rho(0 \text{ K})$ was also observed in $\text{Ba}_{1-x}\text{K}_x\text{Fe}_2\text{As}_2$ [30]. The obtained exponent of $n \sim 1.3$ for $\text{KCa}_2\text{Fe}_4\text{As}_4\text{F}_2$ is a little bit smaller than that of $n \sim 1.4\text{-}2.0$ in $\text{Ba}_{1-x}\text{K}_x\text{Fe}_2\text{As}_2$, which suggests larger T -linear contribution. Instead of the extrapolated $\rho(0 \text{ K})$, the sample quality was evaluated by the resistivity value just above T_c , $\rho(36 \text{ K})$, which is 28.2 and 23.1 $\mu\Omega\text{cm}$ for sample No. 1 and No.2, respectively. With these values of $\rho(36 \text{ K})$, the residual resistivity ratio (RRR) is defined by $\rho(300 \text{ K})/\rho(36 \text{ K})$, resulting to $\text{RRR} \sim 11.4$ or 12.3, respectively. In a similar compound of $\text{CaKFe}_4\text{As}_4$, RRR ($\rho(300 \text{ K})/\rho(35 \text{ K})$) of ~ 15 has been reported [26]. Relatively large RRR, small residual resistivity, and sharp transition width indicate that our crystals are of high quality.

Figures 4(a) and 4(b) show the temperature dependence of ρ_{ab} of sample No.1 sample for $H//c$ -axis and $H//ab$ -plane measured at various magnetic fields up to 50 kOe. As the magnetic field is increased, the superconducting transition for $H//c$ -axis broadens significantly compared with that for $H//ab$ -plane. Two kinds of irreversibility fields, for fields along c -axis (H_{irr}^c) or ab -plane (H_{irr}^{ab}), were also estimated from ρ_{ab} data. They are defined by the criteria of $\rho_{ab} \sim 0.5 \mu\Omega\text{cm}$. Obtained temperature dependences of H_{irr}^c and H_{irr}^{ab} are shown in Fig. 4(c). We also evaluate two kinds of H_{c2} , for fields along c -axis (H_{c2}^c) or ab -plane (H_{c2}^{ab}), by applying the Werthamer-Helfand-Hohenberg (WHH) formula, $H_{c2}(0 \text{ K}) = -0.693T_c dH_{c2}/dT(T = T_c)$ [31], and obtained $H_{c2}(T)$ as shown in Fig. 4(c). H_{c2} is defined by the two different criteria of $0.9\rho_n$ and $0.5\rho_n$. Here, ρ_n is the normal state resistivity estimated from the extrapolation of the resistivity using the power-law form with $n = 1.3$ as shown in the broken line in Fig. 4(a). Estimated $H_{c2}^{ab}(0 \text{ K})$ is 10,820 and 3,012 kOe, and $H_{c2}^c(0 \text{ K})$ is 1,326 and 407 kOe, for $0.9\rho_n$ and $0.5\rho_n$, respectively. Using these data, the anisotropy parameter $\gamma = H_{c2}^{ab}/H_{c2}^c$ is also evaluated as 8.2 and 7.4 for $0.9\rho_n$ and $0.5\rho_n$, respectively. These estimated values of γ and $H_{c2}^{ab}(0 \text{ K})$ are similar to that in the previous report [17], and significantly larger than those of other IBSs [26,32-34].

To discuss the anisotropy of $\text{KCa}_2\text{Fe}_4\text{As}_4\text{F}_2$, we measured ρ_c for sample No. 3 ($520 \times 326 \times 13 \mu\text{m}^3$). A schematic drawing of the electrical contacts attached to $\text{KCa}_2\text{Fe}_4\text{As}_4\text{F}_2$ for ρ_c measurements is shown in Fig. 5(a). Compared with ρ_{ab} , the magnitude and temperature dependence of ρ_c are very different. As shown in Fig. 5(b), the ρ_c at room temperature is 35 $\text{m}\Omega\text{cm}$, which is almost 100 times larger than the value of ρ_{ab} shown in Fig. 3(b). In the simplest scenario, the anisotropy of the resistivity should be equal to γ^2 . ρ_c/ρ_{ab} using the ρ_{ab} of sample No.1 is shown in Fig. 5(c). ρ_c/ρ_{ab} at

room temperature is ~ 100 , which is close to γ^2 evaluated from the anisotropy of H_{c2} . ρ_c/ρ_{ab} increases with decreasing temperature, reaching a very large value of $\sim 1,800$ around T_c . These values are significantly larger than that in doped and non-doped BaFe_2As_2 (~ 100 [34] or ~ 4 [35,36]). The value of ρ_c/ρ_{ab} larger than 100 with increasing trend with decreasing temperature are also observed in cuprate superconductors [37-39] and some IBS compounds such as $(\text{Li}_{0.84}\text{Fe}_{0.16})\text{OHFe}_{0.98}\text{Se}$ [11] and $\text{Li}_x(\text{NH}_3)_y\text{Fe}_2\text{Se}_2$ [12], where highly two-dimensional electronic states are suggested. In $\text{La}_{2-x}\text{Sr}_x\text{CuO}_4$, ρ_c/ρ_{ab} for over-doped with $x \sim 0.3$, where Fermi-liquid like metallic resistivity ($\rho \sim T^\alpha$, $\alpha > 1$) is observed, is almost temperature independent. On the other hand, that for under-doped with $x < 0.2$ increases significantly with decreasing temperature [37], which is similar to that in $\text{KCa}_2\text{Fe}_4\text{As}_4\text{F}_2$. These results can be understood by the quasi two-dimensional Fermi-surface sheets revealed by the first-principles calculations [8,9,13]. Furthermore, temperature dependence of ρ_c shows a broad maximum with its maximum at around 90 K, and a tiny kink just above T_c . Similar behavior is reported in $\text{CsCa}_2\text{Fe}_4\text{As}_4\text{F}_2$ single crystal [18]. A broad maximum in ρ_c - T has also been observed in the same 12442-type of $\text{CsCa}_2\text{Fe}_4\text{As}_4\text{F}_2$ [18], or $(\text{Li}_{0.84}\text{Fe}_{0.16})\text{OHFe}_{0.98}\text{Se}$ [11], and $\text{Li}_x(\text{NH}_3)_y\text{Fe}_2\text{Se}_2$ [12]. This crossover of temperature dependence of ρ_c may suggest opening of pseudogap in $\text{KCa}_2\text{Fe}_4\text{As}_4\text{F}_2$ as suggested by ref. [40-42].

The Hall resistivity ρ_{xx} as a function of magnetic field up to 50 kOe at several temperatures are shown in Fig. 6(a). Dimensions of the sample are $784 \times 730 \times 12 \text{ } \mu\text{m}^3$. In the whole range, ρ_{xx} is positive and shows linear field dependence up to 50 kOe. The Hall coefficient R_H in $\text{KCa}_2\text{Fe}_4\text{As}_4\text{F}_2$ obtained from ρ_{xx} is plotted in Fig. 6(b). The sign of R_H is positive in the whole temperature range, which is consistent with self hole-doping scenario based on the first-principle calculation [13]. R_H increases with decreasing temperature from 300 K to 80 K, and stays nearly constant below 80 K. The absolute value of R_H around T_c is two times larger than that at 300 K. The absolute value of R_H in our single crystal is smaller than that of R_H in polycrystalline sample [6,14]. Around 75 K where R_H takes its maximum value, R_H of single crystal and polycrystalline sample are ~ 1.5 and $2.0 \times 10^{-3} \text{ cm}^3/\text{C}$, respectively. Larger R_H in polycrystalline sample could be originated from the increase of Hall resistivity caused by lower packing density and the anisotropy of the Hall coefficient. The absolute value of R_H at 300 K, $\sim 0.7 \times 10^{-3} \text{ cm}^3/\text{C}$, is similar to that of other IBSs such as $\text{Ba}(\text{Fe}_{1-x}\text{Co}_x)_2\text{As}_2$ ($\sim 1.1 \times 10^{-3} \text{ cm}^3/\text{C}$ for $x = 0.1$) [43], $\text{Ba}_{1-x}\text{K}_x\text{Fe}_2\text{As}_2$ ($\sim 0.5 \times 10^{-3} \text{ cm}^3/\text{C}$ for $x \sim 0.5$) [44] or $\text{CaKFe}_4\text{As}_4$ ($\sim 0.4 \times 10^{-3} \text{ cm}^3/\text{C}$) [26]. It is noteworthy that doped carriers to FeAs layer in $\text{KCa}_2\text{Fe}_4\text{As}_4\text{F}_2$ should be almost the same as those in $\text{Ba}_{0.5}\text{K}_{0.5}\text{Fe}_2\text{As}_2$ and $\text{CaKFe}_4\text{As}_4$, since the number of doped hole per Fe is the same in these three compounds. Similar values of R_H in these compounds are consistent to the simple hole-doping scenario. The temperature dependence of R_H shown in Fig. 6(b) is consistent with a multiband electronic structure of $\text{KCa}_2\text{Fe}_4\text{As}_4\text{F}_2$. In a simple single-band system, the Hall coefficient is given by $R_H = 1/nqc$, where q is the charge of a carrier, n is the carrier density, and c is the speed of light, and R_H is T -independent. By contrast, the Hall

coefficient in a multiband system, for instance, consisting of electron and hole bands, is given by $R_H = (n_h \mu_h^2 - n_e \mu_e^2) / [e((n_h \mu_h + n_e \mu_e)^2)]$, where n_h (n_e) is the density of holes (electrons) and μ_h (μ_e) is the mobility of holes (electrons). The Hall coefficient in a multiband system can be temperature-dependent. The obtained results indicate that $\text{KCa}_2\text{Fe}_4\text{As}_4\text{F}_2$ is a multiband system, which is consistent with the band structure calculation [13].

The J_c in $\text{KCa}_2\text{Fe}_4\text{As}_4\text{F}_2$ was evaluated by measuring the irreversible magnetization. First, in-plane J_c for $H//c$ -axis, which we simply call J_c , was evaluated from magnetization measurements. In the conventional method, J_c can be evaluated using the extended Bean model $J_c = 20\Delta M/a/(1-a/3b)$, where ΔM [emu/cm^3] is $M_{\text{down}} - M_{\text{up}}$. M_{up} and M_{down} are the magnetization when sweeping the field up and down, respectively, and a [cm] and b [cm] are the sample width and length ($a < b$) [45-47]. For some magnetization data, however, since the self-field is significant, ΔM is reduced in the return branch and causes a non-negligible errors in the calculation of J_c . So J_c was calculated from the magnetization of the second quadrant of the magnetic hysteresis loop in Fig. 7(a) using the extended isotropic Bean model, $J_c = 40M_{\text{down}}/a/(1-a/3b)$, after subtracting linear background, as described in ref. [48]. Figure 7 (a) shows the magnetic field dependence of magnetization at various temperatures. Evaluated J_c as a function of temperature is summarized in Fig. 7(b). J_c at 2 K under the self-field is $8.2 \text{ MA}/\text{cm}^2$. This value of J_c is significantly larger than those of other IBSs in the same condition, such as $\text{Ba}(\text{Fe},\text{Co})_2\text{As}_2$ ($1.0 \text{ MA}/\text{cm}^2$) [49], $\text{BaFe}_2(\text{As},\text{P})_2$ ($1.4 \text{ MA}/\text{cm}^2$) [50], $(\text{Ba},\text{K})\text{Fe}_2\text{As}_2$ ($2.4 \text{ MA}/\text{cm}^2$) [51], and $\text{CaKFe}_4\text{As}_4$ ($1.6 \text{ MA}/\text{cm}^2$) [27]. The value of J_c at 20 K under the self-field is $0.38 \text{ MA}/\text{cm}^2$. This value agrees reasonably well with that evaluated from the analysis of the MO image. A slight underestimation of J_c evaluated from MO image may be caused by the effect of observed defect or a slightly larger gap between the sample surface and the garnet film. J_c decreases monotonically with the magnetic field without showing the peak effect in the whole temperature range. At temperatures above 20 K, the magnetic field dependence of J_c becomes significant as shown in Fig. 7(b). This is consistent with the low irreversibility field near T_c as described in Fig. 4(c). Next, we demonstrate further enhancement of J_c by swift-particle irradiation. It is well known that point or columnar defects created by swift-particle irradiation work as pinning centers for vortices and increase J_c [49]. We introduced columnar defects by using 2.6 GeV U-ion irradiation at a dose equivalent field of $B_\phi = 40 \text{ kG}$. The J_c as a function of magnetic field of the $\text{KCa}_2\text{Fe}_4\text{As}_4\text{F}_2$ is summarized in Fig. 8. The J_c in 2.6 GeV U-ion irradiated sample was calculated by the same method for that in the pristine sample. After the irradiation, J_c at 2 K under the self-field is enhanced up to $\sim 19 \text{ MA}/\text{cm}^2$, which is more than twice the value of the pristine crystal. The largest value of J_c obtained at 2 K under self-field in 2.6 GeV U-irradiated $\text{KCa}_2\text{Fe}_4\text{As}_4\text{F}_2$ is slightly larger than those in heavy ion-irradiated $(\text{Ba},\text{K})\text{Fe}_2\text{As}_2$, $\sim 15 \text{ MA}/\text{cm}^2$ [52]. Considering the fact that J_c can be enhanced with adding proper defects as pinning centers by changing conditions of irradiation, further increase of J_c can be expected in $\text{KCa}_2\text{Fe}_4\text{As}_4\text{F}_2$ with artificial defects.

In the case of compounds with tetragonal symmetry, three kinds of J_c should be considered. One of them is in-plane J_c when the field is applied along the c -axis as discussed above. The others are two independent critical current densities for $H//ab$ -plane, one flows in the ab -plane and another flows along the c -axis. We tentatively designate the former as J_{c2} and the latter as J_{c3} (following the definition in ref. [27]). However, it is difficult to evaluate J_{c2} and J_{c3} independently without large difference between J_{c2} and J_{c3} as in the case of $\text{CaKFe}_4\text{As}_4$ [27]. Hence, we only evaluated average J_c for $H//ab$ -plane, $J_c^{H//ab}$, using the extended Bean model. Since the return branch cannot be estimated well due to the small magnetization compared with the background signal, J_c is calculated using the conventional extended Bean model $J_c = 20\Delta M/a(1-a/3b)$. Figure 9(b) shows temperature dependence of $J_c^{H//ab}$ under self-field together with the self-field J_c for $H//c$ -axis. Compared with J_c for $H//c$ -axis, the absolute value of $J_c^{H//ab}$ is smaller, especially below 10 K. The self-field $J_c^{H//ab}$ at 2 K is $\sim 0.9 \text{ MA/cm}^2$. Anisotropic J_c has not been studied properly in other iron-based and even cuprate superconductors. For instance, $\text{Ba}(\text{Fe},\text{Co})_2\text{As}_2$ and $\text{Fe}(\text{Te},\text{Se})$ single crystals are reported to show isotropic J_c [49,53]. On the other hand, $J_c^{H//ab}$ in $\text{CaKFe}_4\text{As}_4$ shows opposite trend ($J_c^{H//ab} > J_c$ for $H//c$ -axis) [54,55], and that in the same 12442-type of $\text{CsCa}_2\text{Fe}_4\text{As}_4\text{F}_2$ at 1.8 K shows similar trend ($J_c^{H//ab} < J_c$ for $H//c$ -axis) [17]. The difference between J_c for $H//c$ -axis and $J_c^{H//ab}$ is shown in Fig. 9(b). J_c under the self-field for $H//c$ -axis is ~ 9 and ~ 1.5 times larger than $J_c^{H//ab}$ at 2 K and above 15 K, respectively. While temperature dependence of $J_c^{H//ab}$ below 10 K is weaker than that of J_c for $H//c$ -axis, values and temperature dependence of both components of J_c become similar above 15 K.

One of the possible reasons for the significantly large and anisotropic J_c could be the presence of natural defects in the pristine $\text{KCa}_2\text{Fe}_4\text{As}_4\text{F}_2$. In the case of $\text{CaKFe}_4\text{As}_4$, where anisotropic J_c was also observed, novel planar defects nearly parallel to the ab -plane were detected by STEM observations [27]. Planar defects can work as pinning centers for vortices, causing enhancement of J_{c2} , or block electrical current flowing along the c -axis leading to reduction of J_{c3} . The former effect may be more dominant in $\text{CaKFe}_4\text{As}_4$. To give a hint for the anisotropic J_c , we performed high-resolution STEM observations. Figures 10(a)-(d) show STEM images on the cross section parallel to the c -axis in the pristine and 2.6 GeV U-irradiated $\text{KCa}_2\text{Fe}_4\text{As}_4\text{F}_2$. Clear periodic structure along the c -axis in Fig. 10 (b) corresponds to half unit cell of $\text{KCa}_2\text{Fe}_4\text{As}_4\text{F}_2$. Horizontal black line-like defects are observed as shown in yellow broken squares in Figs. 10(a), 10(c), and 10(d), respectively. These planar defects extending more than 400 nm are randomly distributed, and the separation between defects is larger than 100 nm. The lower density of defects and longer defects along the ab -plane in $\text{KCa}_2\text{Fe}_4\text{As}_4\text{F}_2$ should reduce J_{c3} effectively rather than increase J_{c2} as opposed to $\text{CaKFe}_4\text{As}_4$, leading to the net reduction of $J_c^{H//ab}$. So the observed defects are possible origin of anisotropic J_c , where $J_c^{H//ab}$ is lower than J_c for $H//c$ -axis. On the other hand, no characteristic defect structure along the c -axis was observed in the pristine $\text{KCa}_2\text{Fe}_4\text{As}_4\text{F}_2$ which may contribute to increase J_c for $H//c$ -axis. Instead, as shown in Fig. 10(b), regions with dark contrasts with 5-10 nm

scale are distributed. They could be the origin of the large $J_c^{H//ab}$ in $\text{KCa}_2\text{Fe}_4\text{As}_4\text{F}_2$. Lattice strains or chemical inhomogeneities of some kind can be the cause of these regions with dark contrasts. On the other hand, in 2.6 GeV U-irradiated $\text{KCa}_2\text{Fe}_4\text{As}_4\text{F}_2$, clear columnar defects along the c -axis are observed as shown in Figs. 10(c) and 10 (d), although these defects look a little discontinuous compared with those in 2.6 GeV U-irradiated K-doped BaFe_2As_2 [48,56]. Possible reason for this difference is that the threshold energies of the irradiated ions to create the continuous columnar defects are different for each material. Actually, it has been confirmed that the continuity and radius of columnar defects are quite different between $\text{Ba}(\text{Fe},\text{Co})\text{Fe}_2\text{As}_2$ and $(\text{Ba},\text{K})\text{Fe}_2\text{As}_2$ irradiated by the same 2.6 GeV U ions [56]. Observed columnar defects should work as pinning center for vortices to increase in-plane J_c as shown in Fig. 8. It should be noted that J_c of the irradiated crystal in higher temperature and magnetic field range shown in Fig. 8 is significantly larger than that of the pristine crystal shown in Fig. 7(b). This indicates that irreversibility field above 20 K is enhanced by pinning of vortices introduced by columnar defect. Higher performance of J_c around 20 K by increasing pinning force is more advantageous for the operation of them using He-free refrigeration systems in future [2]. Moreover, further enhancement of J_c of $\text{KCa}_2\text{Fe}_4\text{As}_4\text{F}_2$ in a wide temperature range is expected. In the case of $\text{Ba}_{0.6}\text{K}_{0.4}\text{Fe}_2\text{As}_2$, degree of enhancement of J_c by heavy-ion irradiation is controlled not only by the matching field, but also by the energy and species of ions [52]. Further enhancement of J_c by controlling the irradiation conditions is demanded in future.

Conclusion

We have presented a systematic study of anisotropic physical properties and critical current density in $\text{KCa}_2\text{Fe}_4\text{As}_4\text{F}_2$. The sharp onset of diamagnetic shielding and the magneto-optical image reveal the homogeneity of single crystal and prominent Bean-like penetrations of vortices. Temperature dependence of ρ_{ab} shows a tendency of saturation at high temperatures with a value $\sim 300 \mu\Omega\text{cm}$ at room temperature. This is comparable to values of $\text{Ba}_{0.5}\text{K}_{0.5}\text{Fe}_2\text{As}_2$ and $\text{CaKFe}_4\text{As}_4$ with similar doping levels, and is consistent to the universality of MIR limit in metals. A large anisotropy of electrical resistivity with $\rho_c/\rho_{ab} \sim 100$ at room temperature and semiconductor-like ρ_c suggest quasi-two-dimensional electronic state. R_H analysis indicates that $\text{KCa}_2\text{Fe}_4\text{As}_4\text{F}_2$ is a multiband system and holes are dominant carriers. The irreversible magnetization reveal significantly larger J_c compared with that in other iron-based superconductors, and large anisotropy of J_c depending on the direction of magnetic field. Origin of anisotropic J_c may be caused by randomly distributed planar defect and scattered dark contrasts as observed in STEM images. Further enhancement of J_c up to 19 MA/cm^2 at 2 K under self-field is also demonstrated by irradiating 2.6 GeV U at $B_\Phi = 40 \text{ kG}$. Significantly large enhancement of J_c is sustained even at high temperatures and high fields.

Acknowledgements

This work was partially supported by a Grant in Aid for Scientific Research (A) (17H01141) from the Japan Society for the Promotion of Science (JSPS).

References

- [1] Y. Watanabe, M. Hirano, and H. Hosono, *J. Am. Chem. Soc.* **130**, 3296 (2008).
- [2] H. Hosono, A. Yamamoto, H. Hiramatsu, and Y. Ma, *Mater. Today* **21**, 278 (2018).
- [3] H. Huang, C. Yao, C. Dong, X. Zhang, D. Wang, Z. Cheng, J. Li, S. Awaji, H. Wen, and Y. Ma, *Supercond. Sci. Technol.* **31**, 015017 (2018).
- [4] S. Pyon, D. Miyawaki, T. Tamegai, S. Awaji, H. Kito, S. Ishida, and Y. Yoshida, *Supercond. Sci. Technol.* **33**, 065001 (2020).
- [5] M. Rotter, M. Tegel, and D. Johrendt, *Phys. Rev. Lett.* **101**, 107006 (2008).
- [6] Z.-C. Wang, C.-Y. He, S.-Q. Wu, Z.-T. Tang, Y. Liu, A. Ablimit, C.-M. Feng, and G.-H. Cao, *J. Am. Chem. Soc.* **138**, 7856 (2016).
- [7] Z. Wang, C. He, Z. Tang, S. Wu, G. Cao, *Sci. China Mater.* **60**, 83 (2017).
- [8] Z.-C. Wang, C.-Y. He, S.-Q. Wu, Z.-T. Tang, Y. Liu, A. Ablimit, Q. Tao, C.-M. Feng, Z.-A. Xu, G.-H. Cao, *J. Phys.: Condens. Matter* **29**, 11LT01 (2017).
- [9] Z.-C. Wang, C.-Y. He, S.-Q. Wu, Z.-T. Tang, Y. Liu, G.-H. Cao, *Chem. Mater.* **29**, 1805 (2017).
- [10] S.-Q. Wu, Z.-C. Wang, C.-Y. He, Z.-T. Tang, Y. Liu, G.-H. Cao, *Phys. Rev. Mater.* **1**, 044804 (2017).
- [11] X. Dong, K. Jin, D. Yuan, H. Zhou, J. Yuan, Y. Huang, W. Hua, J. Sun, P. Zheng, W. Hu, Y. Mao, M. Ma, G. Zhang, F. Zhou, and Z. Zhao, *Phys. Rev. B* **92**, 064515 (2015).
- [12] S. Sun, S. Wang, R. Yu, and H. Lei, *Phys. Rev. B* **96**, 064512 (2017).
- [13] G. Wang, Z. Wang, and X. Shi, *EPL* **116**, 37003 (2016).
- [14] J. Ishida, S. Iimura, H. Hosono, *Phys. Rev. B* **96**, 174522 (2017).
- [15] B. Wang, Z.-C. Wang, K. Ishigaki, K. Matsubayashi, T. Eto, J. Sun, J.-G. Cheng, G.-H. Cao, Y. Uwatoko, *Phys. Rev. B* **99**, 014501 (2019).
- [16] M. Smidman, F. K. K. Kirschner, D. T. Adroja, A. D. Hillier, F. Lang, Z. C. Wang, G. H. Cao, and S. J. Blundell, *Phys. Rev. B* **97**, 060509(R) (2018).
- [17] T. Wang, J. Chu, H. Jin, J. Feng, L. Wang, Y. Song, C. Zhang, X. Xu, W. Li, Z. Li, T. Hu, D. Jiang, W. Peng, X. Liu, and G. Mu, *J. Phys. Chem. C* **123**, 13925 (2019).
- [18] Z.-C. Wang, Y. Liu, S.-Q. Wu, Y.-T. Shao, Z. Ren, and G.-H. Cao, *Phys. Rev. B* **99**, 144501 (2019).
- [19] A. B. Yu, T. Wang, Y. F. Wu, Z. Huang, H. Xiao, G. Mu, and T. Hu, *Phys. Rev. B* **100**, 144505 (2019).
- [20] W. Hong, L. Song, B. Liu, Z. Li, Z. Zeng, Y. Li, D. Wu, Q. Sui, T. Xie, S. Danilkin, H. Ghosh, A. Ghosh, J. Hu, L. Zhao, X. Zhou, X. Qiu, S. Li, and H. Luo, *arXiv:2005.06146v1* (2020).
- [21] H. Q. Yuan, J. Singleton, F. F. Balakirev, S. A. Baily, G. F. Chen, J. L. Luo, and N. L. Wang, *Nature (London)* **457**, 565 (2009).
- [22] M. M. Altarawneh, K. Collar, C. H. Mielke, N. Ni, S. L. Bud'ko, and P. C. Canfield, *Phys. Rev. B* **78**, 220505 (2008).

- [23] Y. Nakajima, Y. Tsuchiya, T. Taen, T. Tamegai, S. Okayasu, and M. Sasase, *Phys. Rev. B* **80**, 012510 (2009).
- [24] Y. Sun, Y. Tsuchiya, S. Pyon, T. Tamegai, C. Zhang, T. Ozaki, and Q. Li, *Supercond. Sci. Technol.* **28**, 015010 (2015).
- [25] M. Nakajima, S. Ishida, T. Tanaka, K. Kihou, Y. Tomioka, T. Saito, C. H. Lee, H. Fukazawa, Y. Kohori, T. Kakeshita, A. Iyo, T. Ito, H. Eisaki, and S. Uchida, *Sci. Rep.* **4**, 5873 (2014).
- [26] W. R. Meier, T. Kong, U. S. Kaluarachchi, V. Taufour, N. H. Jo, G. Drachuck, A. E. Böhmer, S. M. Saunders, A. Sapkota, A. Kreyssig, M. A. Tanatar, R. Prozorov, A. I. Goldman, Fedor F. Balakirev, Alex Gurevich, S. L. Bud'ko, and P. C. Canfield, *Phys. Rev. B* **94**, 064501 (2016).
- [27] S. Pyon, A. Takahashi, I. Veshchunov, T. Tamegai, S. Ishida, A. Iyo, H. Eisaki, M. Imai, H. Abe, T. Terashima, and A. Ichinose, *Phys. Rev. B* **99**, 104506 (2019).
- [28] A. F. Ioffe, and A. R. Regel, *Prog. Semicond.* **4**, 237(1960).
- [29] N. E. Hussey, K. Takenaka, and H. Takagi, *Phil. Mag.* **84**, 2847 (2004).
- [30] Y. Liu, M. A. Tanatar, W. E. Straszheim, B. Jensen, K. W. Dennis, R. W. McCallum, V. G. Kogan, R. Prozorov, and T. A. Lograsso, *Phys. Rev. B* **89**, 134504 (2014).
- [31] N. R. Werthamer, E. Helfand, and P. C. Hohenberg, *Phys. Rev.* **147**, 295 (1966).
- [32] Y. Jia, P. Cheng, L. Fang, H. Luo, H. Yang, C. Ren, L. Shan, C. Gu, and H.-H. Wen, *Appl. Phys. Lett.* **93**, 032503 (2008).
- [33] Z.-S. Wang, H.-Q. Luo, C. Ren, and H.-H. Wen, *Phys. Rev. B: Condens. Matter Mater. Phys.* **78**, 140501(R) (2008).
- [34] X. F. Wang, T. Wu, G. Wu, H. Chen, Y. L. Xie, J. J. Ying, Y. J. Yan, R. H. Liu, and X. H. Chen, *Phys. Rev. Lett.* **102**, 117005 (2009).
- [35] M. A. Tanatar, N. Ni, G. D. Samolyuk, S. L. Bud'ko, P. C. Canfield, and R. Prozorov, *Phys. Rev. B* **79**, 134528 (2009).
- [36] M. A. Tanar, M. S. Torikachvili, A. Thaler, S. L. Bud'ko, P. C. Canfield, and R. Prozorov, *Phys. Rev. B* **90**, 104518 (2014).
- [37] Y. Nakamura, and S. Uchida, *Phys. Rev. B* **47**, 8369 (1993).
- [38] K. Takenaka, K. Mizuhashi, H. Takagi, and S. Uchida, *Phys. Rev. B* **50**, 6534 (1994).
- [39] T. Watanabe, T. Fujii, and A. Matsuda, *Phys. Rev. Lett.* **79**, 2113 (1997).
- [40] M. A. Tanatar, N. Ni, A. Thaler, S. L. Bud'ko, P. C. Canfield, and R. Prozorov, *Phys. Rev. B* **82**, 134528 (2010).
- [41] M. A. Tanatar, N. Ni, A. Thaler, S. L. Bud'ko, P. C. Canfield, and R. Prozorov, *Phys. Rev. B* **84**, 014519 (2011).
- [42] M. A. Tanatar, E. C. Blomberg, H. Kim, K. Cho, W. E. Straszheim, B. Shen, H.-H. Wen, and R. Prozorov, *arXiv:1106.0533* (2011).
- [43] Y. Nakajima, T. Taen, and T. Tamegai, *J. Phys. Soc. Jpn.* **78**, 023702 (2009).

- [44] K. Ohgushi, and Y. Kiuchi, Phys. Rev. B **85**, 064522 (2012).
- [45] Y. Nakajima, Y. Tsuchiya, T. Taen, T. Tamegai, S. Okayasu, and M. Sasase, Phys. Rev. B **80**, 012510 (2009).
- [46] C. P. Bean, Rev. Mod. Phys. **36**, 31 (1964).
- [47] E. M. Gyorgy, R. B. van Dover, K. A. Jackson, L. F. Schneemeyer, and J. V. Waszczak, Appl. Phys. Lett. **55**, 283 (1989).
- [48] A. Park, S. Pyon, K. Ohara, N. Ito, and T. Tamegai, Phys. Rev. B **97**, 064516 (2018).
- [49] T. Tamegai, T. Taen, H. Yagyuda, Y. Tsuchiya, S. Mohan, T. Taniguchi, Y. Nakajima, S. Okayasu, M. Sasase, H. Kitamura, T. Murakami, T. Kambara, and Y. Kanai, Supercond. Sci. Technol. **25**, 084008 (2012).
- [50] A. Park, I. Veshchunov, A. Mine, S. Pyon, T. Tamegai, and H. Kitamura, accepted in Phys. Rev. B.
- [51] T. Taen, F. Ohtake, S. Pyon, T. Tamegai, and H. Kitamura, Supercond. Sci. Technol. **28**, 085003 (2015).
- [52] F. Ohtake, T. Taen, S. Pyon, T. Tamegai, S. Okayasu, T. Kambara, and H. Kitamura, Physica C **518**, 47 (2015).
- [53] Y. Sun, T. Taen, Y. Tsuchiya, Q. Ding, S. Pyon, Z. Shi, and T. Tamegai, Appl. Phys. Express **6**, 043101 (2013).
- [54] S. J. Singh, M. Bristow, W. R. Meier, P. Taylor, S. J. Blundell, P. C. Canfield, and A. I. Coldea, Phys. Rev. Mater. **2**, 074802 (2018).
- [55] S. Ishida, A. Iyo, H. Ogino, H. Eisaki, N. Takeshita, K. Kawashima, K. Yanagisawa, Y. Kobayashi, K. Kimoto, H. Abe, M. Imai, J. Shimoyama, and M. Eisterer, npj Quantum Materials **4**, 27 (2019).
- [56] N. Ito, S. Pyon, T. Kambara, A. Yoshida, S. Okayasu, A. Ichinose, and T. Tamegai, J. Phys.: Conf. Series **1054**, 012020 (2018).

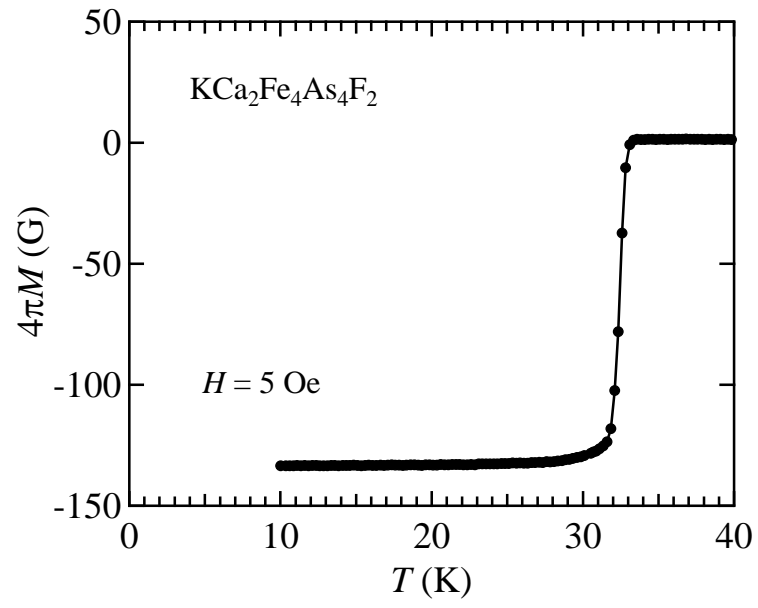


Fig. 1. Temperature dependence of the zero-field-cooled magnetization at $H = 5$ Oe along the c -axis in $\text{KCa}_2\text{Fe}_4\text{As}_4\text{F}_2$.

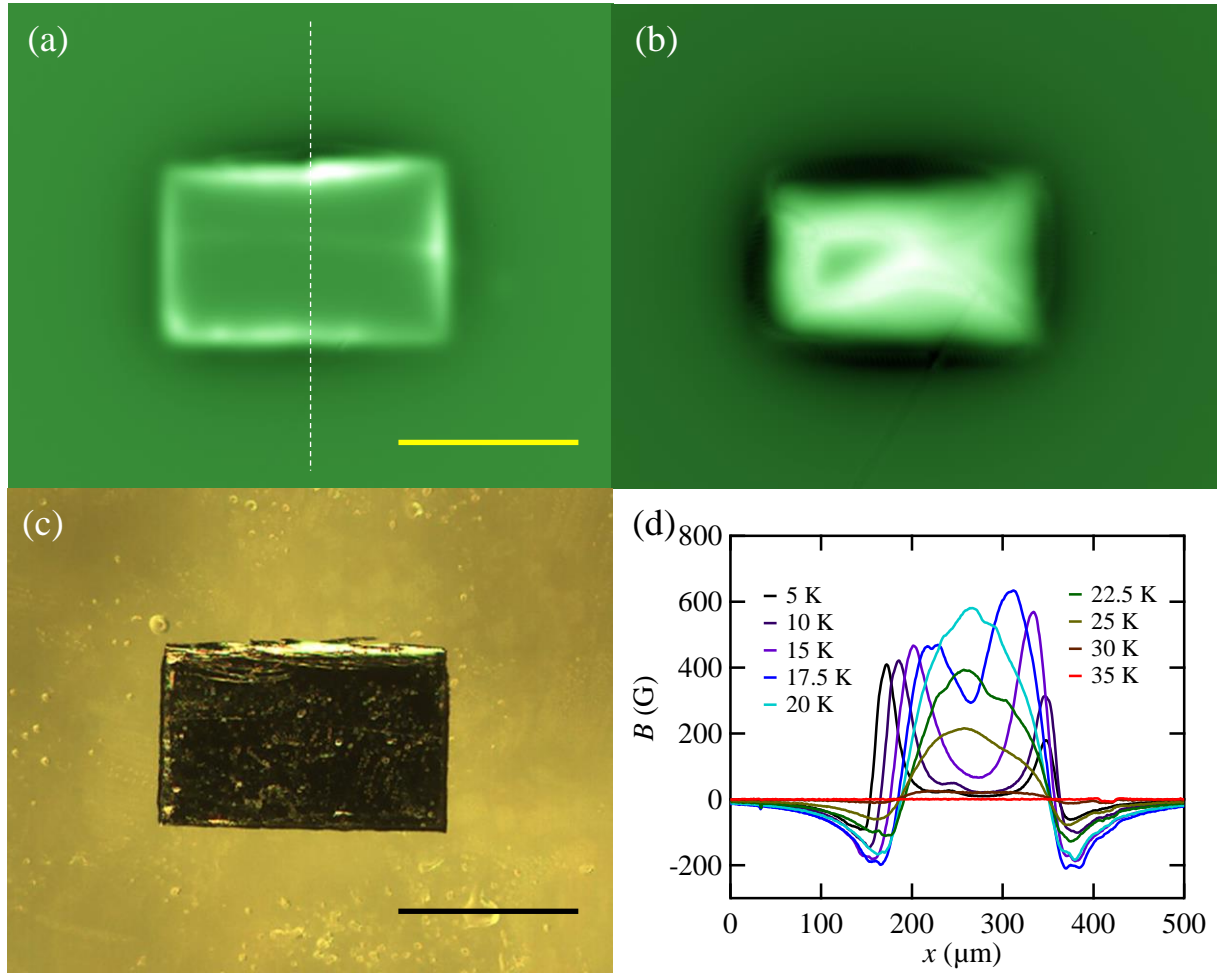


Fig. 2. Differential MO images of $\text{KCa}_2\text{Fe}_4\text{As}_4\text{F}_2$ in the remanent state at (a) 5 K and (b) 20 K after cycling the field up to 1.6 kOe for 0.2 s. (c) An optical micrograph of $\text{KCa}_2\text{Fe}_4\text{As}_4\text{F}_2$. (d) Local magnetic induction profiles at different temperatures taken along the broken line in (a). Both the yellow bar in (a) and black bar in (c) correspond to 200 μm .

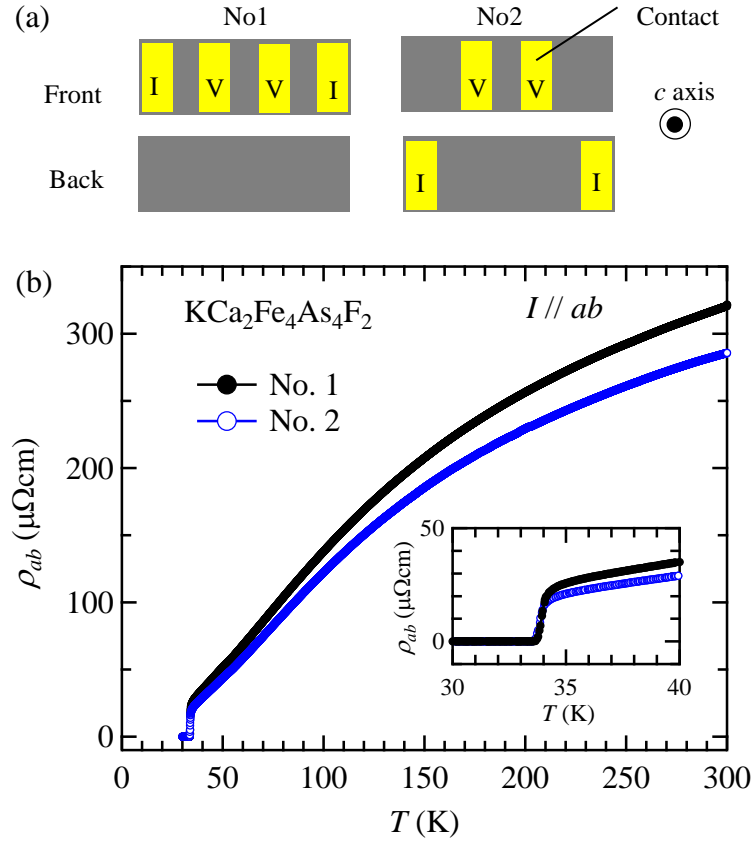


Fig. 3 (a) Schematic drawings of the two samples with electrical contacts for measurements of in-plane electrical resistivity (ρ_{ab}). (b) Temperature dependence of ρ_{ab} in $\text{KCa}_2\text{Fe}_4\text{As}_4\text{F}_2$ sample No. 1 and No. 2 measured in a temperature range of 30-300 K. The inset in (b) shows $\rho_{ab} - T$ near T_c .

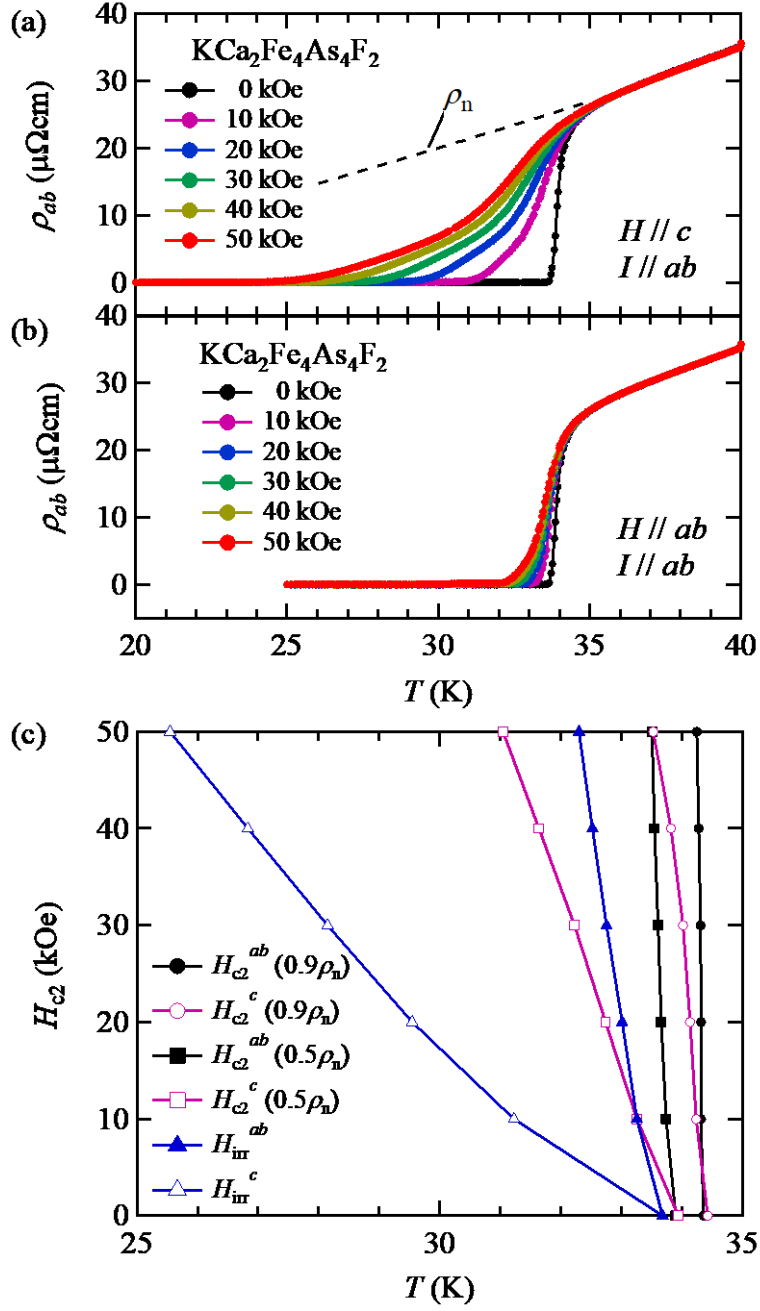


Fig. 4. Temperature dependence of in-plane electrical resistivity (ρ_{ab}) in $\text{KCa}_2\text{Fe}_4\text{As}_4\text{F}_2$ (No.1) below 40 K under various magnetic fields parallel to the (a) c -axis and (b) ab -plane. (c) Anisotropic H_{c2} and H_{irr} evaluated from temperature-dependent resistivity in (a) and (b). H_{c2} is defined by two different criteria of $0.9\rho_n$ and $0.5\rho_n$. Here, ρ_n is the normal state resistivity estimated from the extrapolation of the resistivity using the power-law form with $n = 1.3$ as shown in the broken line in (a). H_{irr} is defined by the criteria of $\rho_{ab} \sim 0.5 \mu\Omega\text{cm}$.

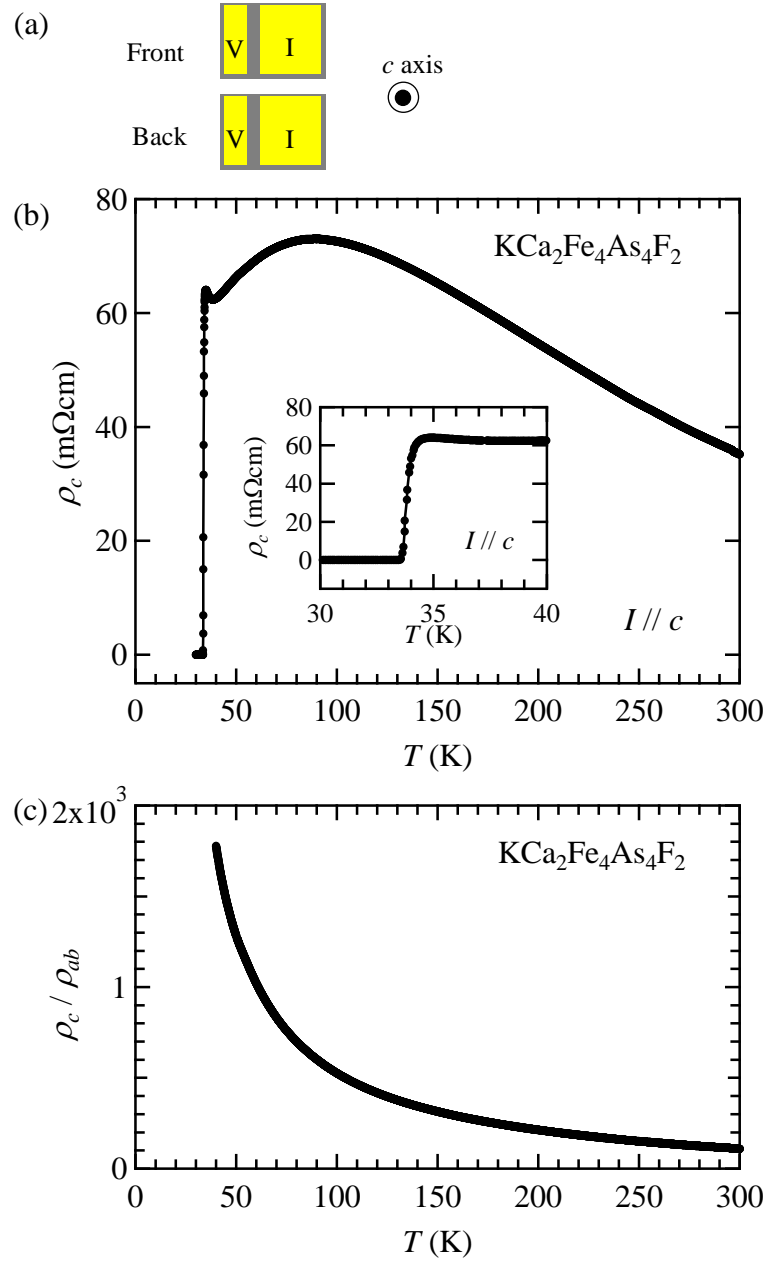


Fig. 5. (a) Schematic drawings of the electrical contacts for the measurement of out-plane electrical resistivity (ρ_c). (b) Temperature dependence of ρ_c in $\text{KCa}_2\text{Fe}_4\text{As}_4\text{F}_2$ in a temperature range of 30-300 K under zero magnetic field. The inset in (b) shows ρ_c - T near T_c . (c) Temperature dependence of the anisotropy of the resistivity, ρ_c / ρ_{ab} . ρ_{ab} of sample No.1 shown in Fig. 3 (b) is used for the calculation.

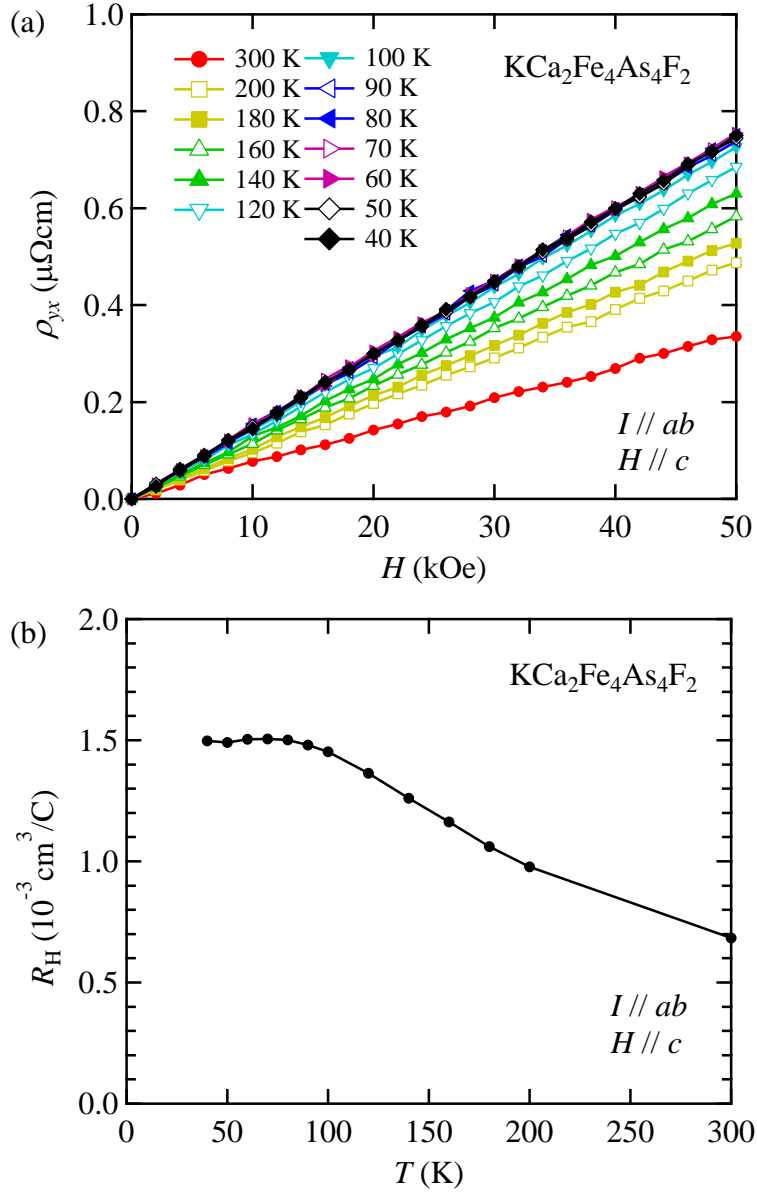


Fig. 6. (a) Hall resistivity ρ_{yx} as a function of field at various temperatures in $\text{KCa}_2\text{Fe}_4\text{As}_4\text{F}_2$. (b) Temperature dependence of the Hall coefficient R_H in $\text{KCa}_2\text{Fe}_4\text{As}_4\text{F}_2$.

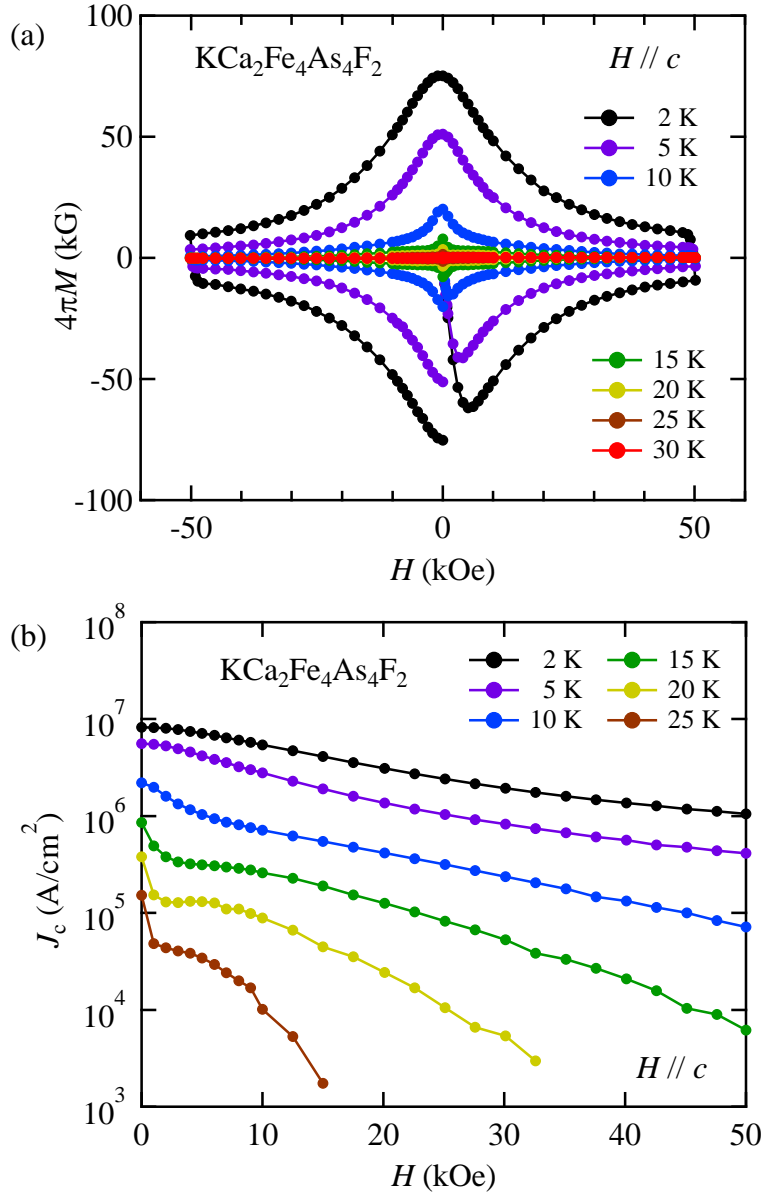


Fig. 7. (a) Magnetic field dependence of magnetization in $\text{KCa}_2\text{Fe}_4\text{As}_4\text{F}_2$ at various temperatures for $H//c$ -axis. (b) Magnetic field dependence of in-plane J_c evaluated using the data shown in (a).

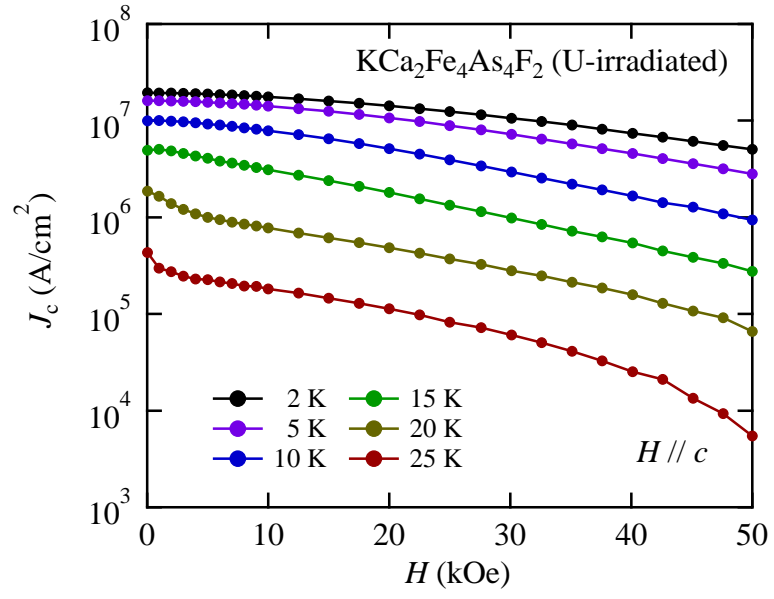


Fig. 8. Magnetic field dependence of magnetic J_c at various temperature in 2.6 GeV U-irradiated ($B_\phi = 40$ kOe) $\text{KCa}_2\text{Fe}_4\text{As}_4\text{F}_2$.

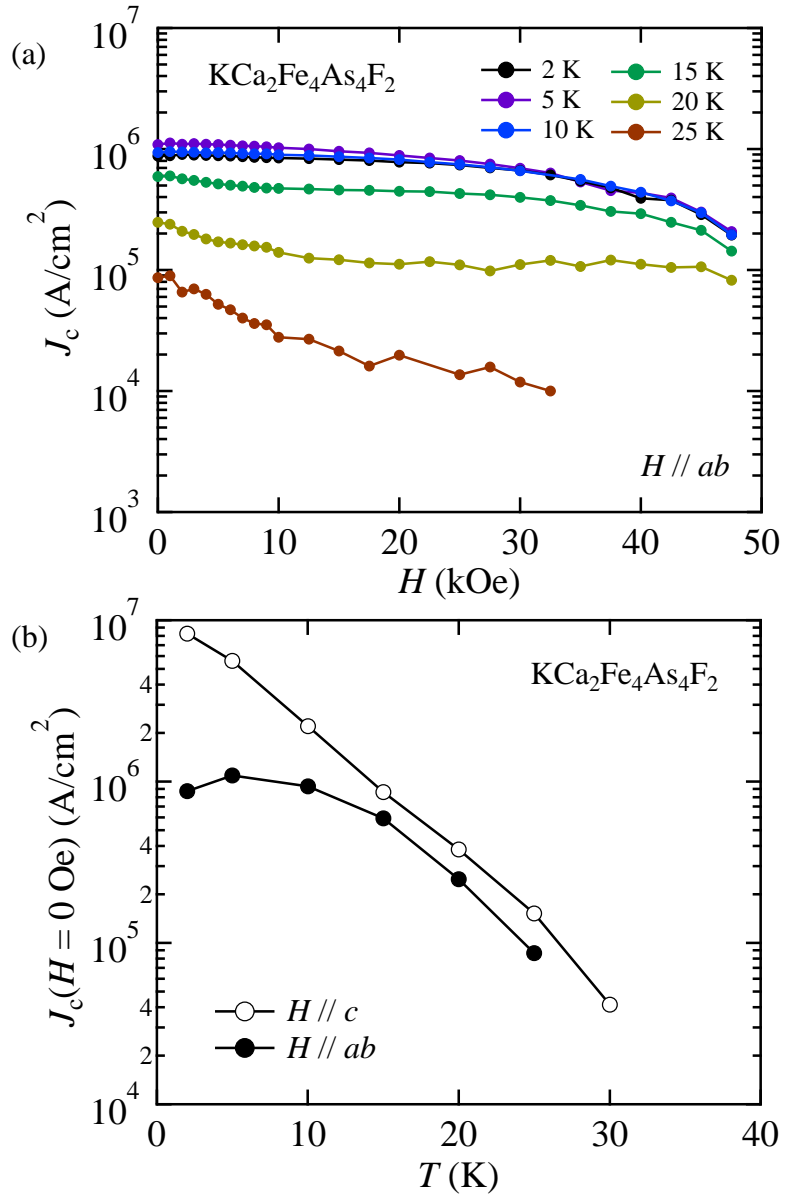


Fig. 9. (a) Magnetic field dependence of magnetic J_c in $\text{KCa}_2\text{Fe}_4\text{As}_4\text{F}_2$ at various temperatures for $H//ab$ -plane. (b) Temperature dependence of magnetic J_c under the self-field in $\text{KCa}_2\text{Fe}_4\text{As}_4\text{F}_2$ for $H//c$ -axis and $H//ab$ -plane.

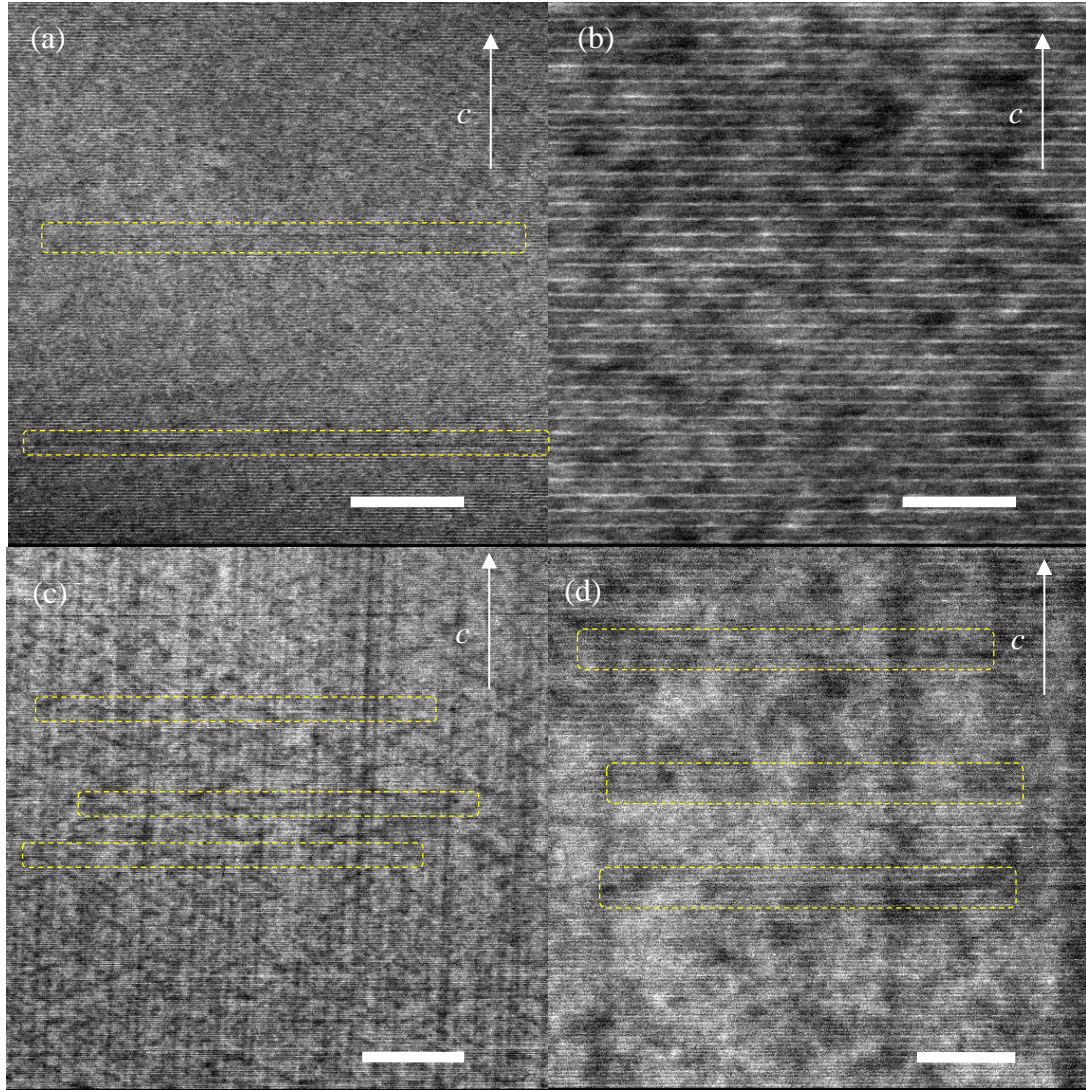


Fig. 10. STEM images of (a), (b) the pristine and (c), (d) 2.6 GeV U-irradiated $\text{KCa}_2\text{Fe}_4\text{As}_4\text{F}_2$ for an electron beam injected along the a axis. Solid lines in (a)-(d) correspond to 100, 10, 100, and 20 nm, respectively. Yellow broken squares in (a), (c), (d) emphasize the location of horizontal black line-like defects.